Experimental study of a wave energy conversion system to equip a self-powered oceanographic buoy

Ricardo Jorge Chaves Andrade
ricardoandrade@tecnico.ulisboa.pt

Instituto Superior Técnico, Universidade de Lisboa, Portugal

June 2018

Abstract

The development of self-powered buoys equipped with data acquisition sensors suggests a new trend around the ocean monitoring technology domain. A buoy capable of extracting energy from waves and, at the same time, provide continuous and real-time data acquisition announces a new generation of oceanographic buoys. Its benefits range from the costs reduction due to less maintenance needed to the possibility of longer periods of ocean deployment, compared to conventional systems including solar modules and batteries for energy storage. For this reason, the cooperation in a single project between IDMEC/IST and DOP/UAz aims to design and deploy for the first time in the open ocean a new generation of self-powered oceanographic buoys equipped with data acquisition sensors. This consortium indicates a significant effort for the development of regional, national and international integrated data systems in the continuous and long-term oceanographic observation. The buoy will be deployed next to the submarine mount Condor at the Azores archipelago (Portugal), for an intended period of one year. This paper describes the conception of a electromechanical system for the oceanographic buoy, as well as the construction and assembly of a prototype to be tested at the IST variable flow turbine test rig.

Keywords: Self-powered oceanographic buoy, oceanographic monitoring, grid-isolated system, oscillating water column, bi-radial turbine, wave energy.

1. Introduction

The development and promotion of new marine monitoring technologies and the reduction of costs in the acquisition of oceanographic data have been priorities of the European Union (EU) [1]. Thus, it is crucial to stimulate technological innovation in oceanographic monitoring systems, as well as to foster new generation technologies, promoting synergies between energy, oceanography and sustainability.

Current oceanographic monitoring technologies still present a number of problems and limitations related to the high cost and size of sensors, very expensive and often non-rechargeable batteries and the low power and reliability of solar modules and wind turbines for the production of electricity. Thus, the solution to these technological constraints may be sought in the adoption of new generation technologies that involve the use of wave energy, the use of autonomous underwater vehicles (AUVs), the improvements to energy storage units and of data acquisition, storage and transmission systems. AUVs provide high versatility of seabed operation and significant cost savings when compared to the use of ships for the same type of studies. However, they face two major problems: low autonomy and difficulty in transmitting data to land. These limitations can be overcome by the development of remote electric charging and information transmission systems that, strategically positioned, could support AUVs. These remote systems could be buoys equipped with wave energy conversion and electrical storage technologies capable of supplying power to various types of oceanographic monitoring sensors and further recharging and collecting/transmitting information to AUVs. In this way, less human intervention is guaranteed at the site and an increase in the time of the oceanographic missions to be carried out with the AUVs is provided, reducing drastically the costs of collecting information.

In this paper firstly it is presented the purpose of the design of the oceanographic buoy and the characteristics that will dictate the system to be used in the experimental tests.

Secondly the electromechanical system chosen for the representation of the buoy is described, so that it is possible to simulate and evaluate its operation in the laboratory.

Next, the design and construction of the experimental installation are described.

Finally, the results of the steady-state and variable flow conditions studied are presented.

2. Wavebuoy - an oceanographic buoy self-powered by wave energy

The buoy has a system that converts wave energy into electrical energy using the oscillating water column (OWC) technology and, when operating as an isolated system of the electric grid, the following elements must be present: air chamber, air turbine, duct for water inlet and outlet, electric generator, batteries, floats and moorings [2]. Apart from this, the buoy also has data acquisition systems (sensors) and communication systems to land.

2.1. Buoy OWC technology

The buoy acts as a partially submerged structure and is composed of an inlet below the water line and a connected air chamber, causing a volume of air above the water line within that chamber. The oscillating motion of the water line present within the structure will promote a reversible airflow through a turbine connected to an electric generator and electric storage batteries [3] (see Fig. 1). The electromechanical system of the buoy will consist of a bi-radial fixed blade turbine [4], an electric generator, a bank of batteries and all the elements of consumption.

Tab. 1 depicts all the elements of consumption of the buoy and electrical power consumption associated with each type of equipment. It should be noted that the total consumption of the equipment is approximately 360 W and that it will have to be ensured uninterrupted by the generator and batteries.

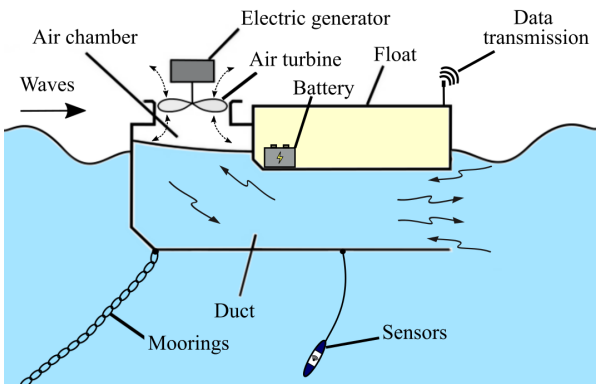

Figure 1: Scheme of oceanographic buoy with OWC technology.

Table 1: Oceanographic buoy power requirements.

Equipment	Power [W]
Oceanographic sensors	10
Valve control	20
Signal lamp	100
Data transmission	20
Data storage	110
Operation measurement	100
Total	360

2.2. Electromechanical modelling of the oceanographic buoy

In order to replicate in the laboratory the electromechanical system of the oceanographic buoy shown in Fig. 1, a diagram was drawn up to illustrate and interconnect its main components. Fig. 2 shows the actual system of the buoy, and Fig. 3 shows the two test models adopted in the experiments. The installation of the electric machines laboratory is out of the scope of this paper, thus only the 55 kW turbines testing laboratory installation and results will be presented here.

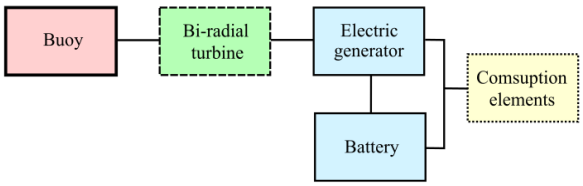

Figure 2: Real electromechanical system of the oceanographic buoy.

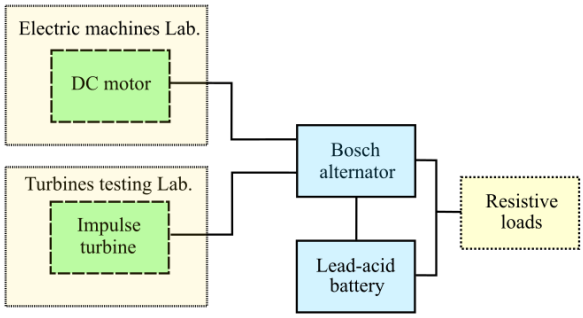

Figure 3: Representative testing models of the electromechanical system of the oceanographic buoy.

3. Experimental model analysis

3.1. Description of the installation

The variable flow test rig used for the experiments is directed to test self-rectifying air turbines in steady-state and variable unidirectional flow conditions (see Fig. 4).

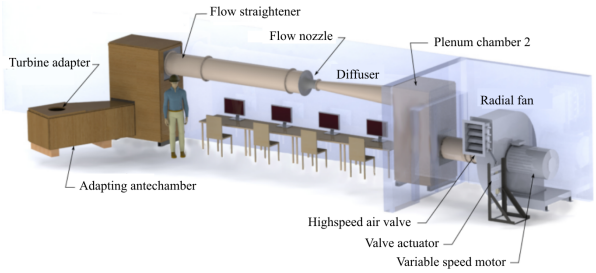

Figure 4: Variable flow test rig of IST [5].

The adaptation chamber (2), coupled to the plenum chamber 1 (3), enables the mounting of vertical axis turbines in a more efficient way. In the present paper, the turbine has a horizontal axis and is connected directly to the plenum chamber 1 and the hole in the adaptation chamber is closed. The plenum chamber 1 allows the uniformization and deceleration of the flow for the entrance of this one into a duct composed of a honeycomb structure. This structure removes vorticity to the flow and aligns it to its entrance in a converging nozzle (5) where the flow rate is measured. Next, there is a diffuser (6) designed to recover the kinetic energy, which in turn is connected to a second plenum chamber (7). This plenum acts as a protection by smoothing out the pressure waves that can be produced by the rapid closing of the air valve (10) downstream. A 55 kW fan (8) is connected to the plenum chamber 2 through a constant diameter pipe and causes the pressure drop in the installation. This fan is driven by a motor (9) which is controlled by a frequency inverter with two quadrants. Finally, downstream of the blower is the air outlet opening to the atmosphere, which contains the air valve connected to an actuator (11).

In this facility there were performed experiments in runaway conditions and in steady-state and variable flows conditions.

4. Results

In this section the results of the tests made in the variable flow test rig will be presented (see Fig. 5). The equivalent circuit of the installation is presented in Fig. 6.

4.1. Steady-state flow conditions

Given the practical impossibility of carrying out tests with various states of charge, it was stipulated that the battery would always have its charge state at 100%, i.e. always fully charged. It was always ensured that the battery did not discharge and that the load current, I_{load}, would never exceed the current produced by the generator I_{ger}. Thus, as the addition of loads requiring more current was tested,

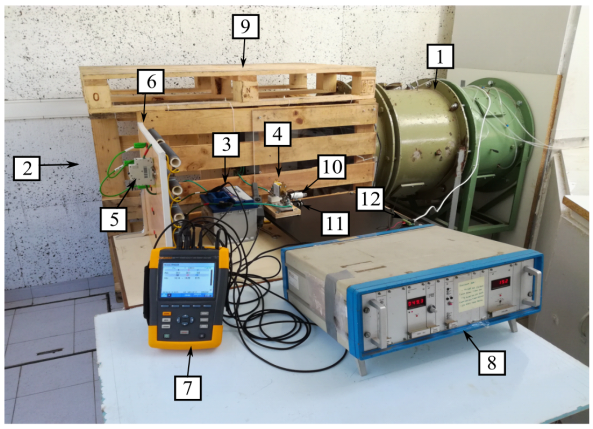

(a) (1) turbine, (2) generator, (3) battery, (4) fuse, (5) circuit breaker, (6) resistive load bank, (7) power analyser FLUKE, (8) data treatment and power system of torque and rotational speed sensor, (9) improved wood and acrylic protection, (10) lamp, (11) switch, (12) *ethernet* cable for torque and rotational speed data transfer.

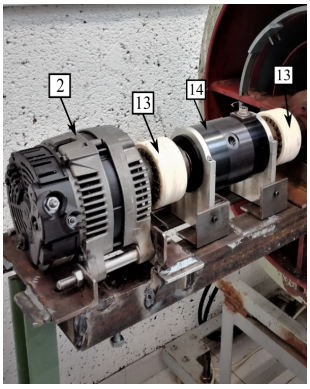

(b) (2) generator, (13) elastic couplings, (14) torque and rotational speed sensor.

Figure 5: Experimental installation.

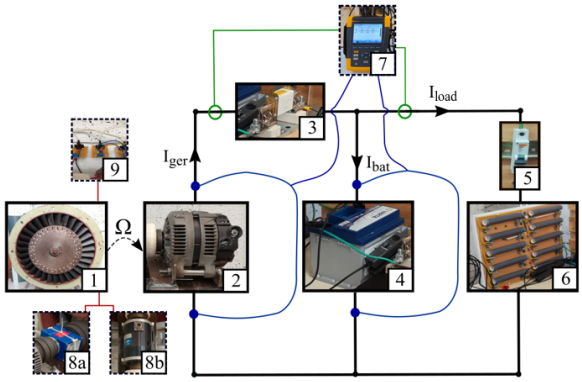

Figure 6: Equivalent circuit of steady-state and variable flow conditions: (1) axial impulse turbine, (2) generator, (3) fuse, (4) battery, (5) circuit breaker, (6) resistive load bank, (7) power analyser FLUKE, (8a and 8b) torque and rotational speed sensors RWT411-DE-KB and TG-5/BP, respectively, (9) pressure sensors.

the tests had to be started at the higher rotational speeds, translating into higher values of I_{ger}. The values of the graph legend to be shown below represent the rated power of the load of each test, the values of 180, 360, 540, 720 and 900 W correspond to the use of an equivalent load resistance of 0.8, 0.4, 0.27, 0.2 and 0.16 Ω.

4.1.1 Turbine operating curves

The control of the generator electromagnetic torque is based on the angular momentum balance

$$T_{\text{aero}}(t) - T_{\text{ger}}(t) - T_{\text{a}}(t) = I\frac{\mathrm{d}\Omega}{\mathrm{d}t}, \tag{1}$$

where I is the rotor inertia of the turbine, Ω the rotational speed, T_{aero} the aerodynamic torque of the turbine, T_{ger} the torque of the generator and T_{a} the friction torque, all in function of time t. In steady-state conditions, with zero acceleration, the rotational speed is constant, thus Eq. (1) can be written as

$$T_{\text{ger}}(t) = T_{\text{aero}}(t) - T_{\text{a}}(t). \tag{2}$$

For the analysis of the results, the dimensional analysis is used [6]. Let the pressure, flow and power coefficients and efficiency be defined respectively by

$$\Psi = \frac{\Delta p_0}{\rho\Omega^2 D^2}, \tag{3}$$

$$\Phi = \frac{Q_{\text{t}}}{\Omega D^3}, \tag{4}$$

$$\Pi = \frac{P_{\text{aero}}}{\rho\Omega^3 D^5}, \tag{5}$$

$$\eta_{\text{turb}} = \frac{\Pi}{\Phi\Psi}. \tag{6}$$

where Δp_0 corresponds to the pressure difference between the atmospheric pressure and the pressure in the plenum chamber, Q_{t} the flow through the turbine, P_{aero} the aerodynamic power ρ the air density and D the turbine diameter.

Fig. 7 illustrates the relationship between the turbine efficiency and the flow coefficient.

The maximum efficiency obtained is approximately 53%, for a flow coefficient value Φ of 0.072. Recall that below 900 r.p.m. the generator is not able to charge the battery. On the other hand, from 2500 r.p.m. the structure of the turbine presented vibrations that could in the long run make the remaining tests infeasible. Hence, the range of pressure coefficients was limited and a complete characterization of the turbine curves was not possible. It was found that regardless of the resistive load applied, the values had an appreciable adjustment, demonstrating that the dimensional analysis was well performed.

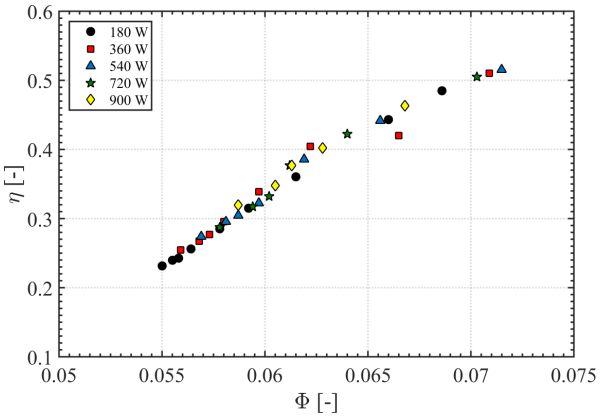

Figure 7: Turbine efficiency vs flow coefficient for different load values.

4.1.2 Generator operating curves

In order to characterize the electrical circuit system, three points were considered such as the generator, battery and load. In these points it were recorded values of current I_{ger} and I_{load}, voltage V_{ger} and V_{bat}, followed by the electric power P_{ger}, P_{bat} and P_{load}. The current direction generator-battery and generator-load were considered positive.

According to the Kirchhoff's current law [7], the battery current is given by

$$I_{\text{bat}} = I_{\text{ger}} - I_{\text{load}}. \tag{7}$$

At each point the electric power is given by

$$P = VI. \tag{8}$$

In order to evaluate the generator operating curves, the values of torque, current, voltage and electrical power were analysed with respect to the generator's rotational speed and imposed resistive load.

The generator only begins to produce current when the rotational speed approaches 900 r.p.m., and for this current to exceed the load current (in order to keep the battery charged) it was necessary to start the tests speeds approximately equal to 1000 r.p.m..

Fig. 8 illustrates the relationship between the generator torque, rotational speed and applied resistive load. The generator torque increases with the increase of the resistive load applied and decreases with the increase of the rotational speed. This is because, for a constant electrical power (due to the fact that the battery is fully charged) when the rotational speed increases, the electromagnetic torque of the generator must necessarily decrease. The percentage change between the initial and final values of the torque was 50, 45, 44, 43, 39 and 29 % respectively for load values equal to 180, 360,

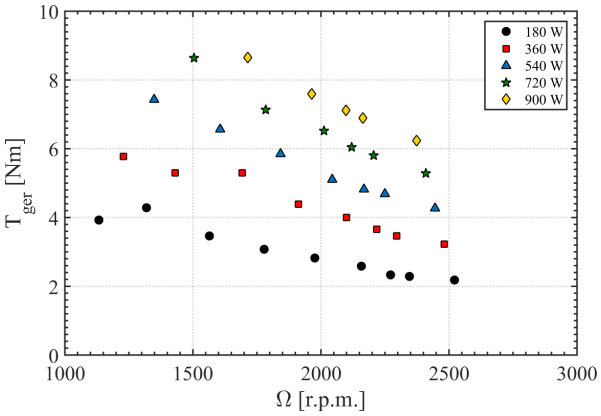

Figure 8: Generator torque vs rotational speed for different load values.

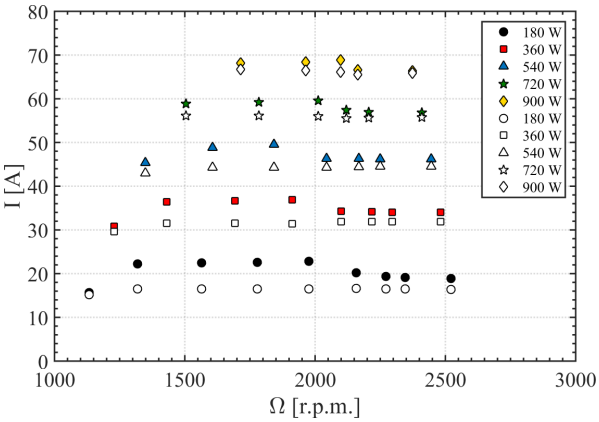

Figure 10: Generator and load currents vs rotational speed for different load values (full symbols: I_{ger}; empty symbols: I_{load}).

540, 720 and 900 W. It is observed that for a same air flow, with the increase of the resistive load, an increase of the electromagnetic torque of the generator is given, which translates into a smaller rotational speed of the turbine.

Fig. 9 shows the relationship between the generator electric power, rotational speed and imposed resistive load. Regardless of the applied load, the power increases to about 1500 r.p.m., keeping constant up to 2000 r.p.m.. Speed from which the power decreases (approximately 50 W), remaining constant up to the maximum speed studied. It was not possible to explain the reason why the power decreases above 2000 r.p.m.. For rotational speeds greater than 1500 r.p.m., the electrical power increase was 40, 25, 20 and 15%, respectively between 180 and 360 W, 360 and 540 W, 540 and 720 W and 720 and 900 W.

Fig. 10 reflects the relationship between the generator current, rotational speed and the load current. As the load increases, the load current has a 50, 35, 20 and 15% percent increase over the previously imposed value. This increased load also provides a higher current output from the generator. The current of the generator has a behaviour similar to that observed in Fig. 9 with respect to the power of the generator. The load current varied approximately between 15 and 67 A while the generator current ranged between 20 and 70 A, respectively for load values of 180 and 900 W. The generator current decreases slightly above 2000 r.p.m., representing a range from 2 to 4 A. It should be noted that a difference is observed between the current of the generator and the current of the load, evidencing that the battery is being overcharged. It is seen that this overcharging current decreases with the increase of the load imposed and takes lower values for the tests above 2000 r.p.m.. However, up to 2000 r.p.m., the percent difference between the value of the generator current and the load current is 30, 16, 10, 5 and 3% relative to the load values of 180, 360, 540, 720 and 900 W.

Fig. 11 reflects the voltage variation of the generator and battery. It has been found that between

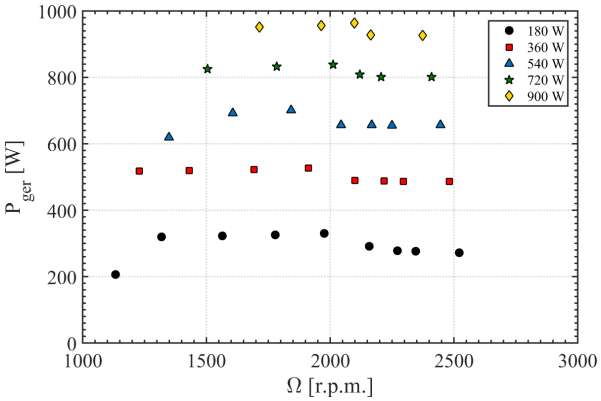

Figure 9: Generator electric power vs rotational speed for different load values.

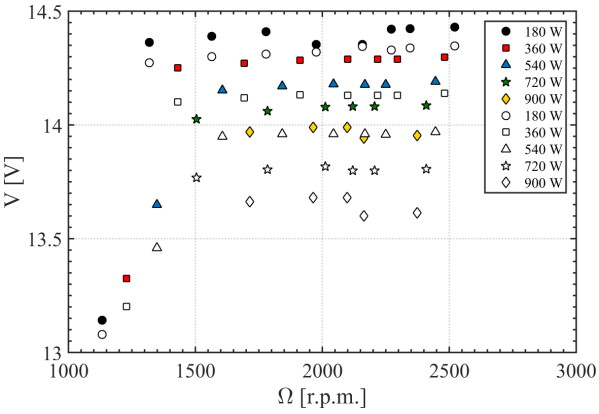

Figure 11: Generator and battery voltage vs rotational speed for different load values (full symbols: V_{ger}; empty symbols: V_{bat}).

1000 and 1500 r.p.m., the voltage increased. For higher rotational speeds, the voltage remained constant. On the other hand, it observed that the difference between the voltage values of the generator and the battery increases with the imposed resistive load. However, this difference can be considered negligible, since the variation is only 0.1 and 0.4 V.

Fig. 12, shows the generator efficiency for steady-state flow conditions. The generator efficiency is

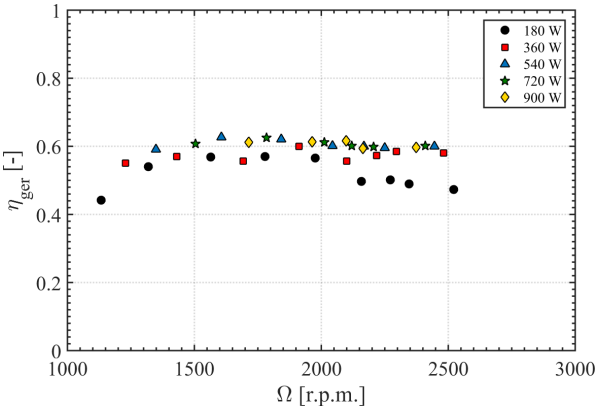

Figure 12: Generator efficiency vs rotational speed for different load values.

given by

$$\eta_{\text{ger}} = \frac{P_{\text{ger}}}{P_{\text{mec}}}, \tag{9}$$

where $P_{\text{mec}} = \Omega T_{\text{ger}}$. The behaviour of the variation of efficiency as a function of the rotational speed, is similar regardless of the load value applied. The maximum efficiency value reached was 65% and occurred in the range of 1500 to 2000 r.p.m.. The efficiency decreases marginally at rotational speeds above 2000 r.p.m., due to the current decrease discussed earlier in Fig. 10.

4.2. Variable flow conditions

In this section will be presented the results obtained in variable flow conditions, for three different sea states,EM1, EM2 and EM3, and with two states of charge of the battery, fully charged and half charged. The most energetic seat state is the EM3 and the less energetic is the EM1. The frequency of occurrence of the following variables was evaluated: P_{ger}, P_{bat}, P_{load}, T_{ger}, and Ω; and the evolution of the following variables was temporarily explained: Δp_0, Q_{t}, P_{avai}, Ω, T_{ger}, P_{ger}, P_{bat} and P_{load}.

4.2.1 Frequency of occurrence analysis

Figs. 13 and 14 shows the frequency of occurrence of the generator electric power, P_{ger}. With the battery charged it is visible that regardless of the sea state, the power of the generator has a peak at 500 W. This value comes from the combined consumption of the load and the battery. The frequency of occurrence of the peak increases gradually with the increase of the power available in each sea state. The peak power was higher for the less energetic sea state, because the battery discharged more time, implying an increase of the power of the generator. The frequency of occurrence at lower values of electric power increases as the sea state presents less available energy. It is highlighted the case of EM1, where the values are distributed uniformly from 250 to 450 W, whereas in EM2 and EM3 the frequency of occurrence for this range of values is almost nil.

Regarding the situation with the half-charged battery, there is a large difference in the values of P_{ger}. These increase significantly with the increase of the value of P_{avai} according to the sea state and present more distributed peaks compared to the first situation (charged battery). In the case of EM1, the values with the highest frequency of

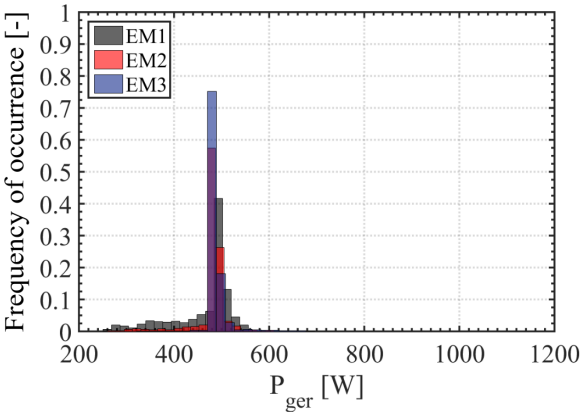

Figure 13: Frequency of occurrence of generator electric power for fully charged battery.

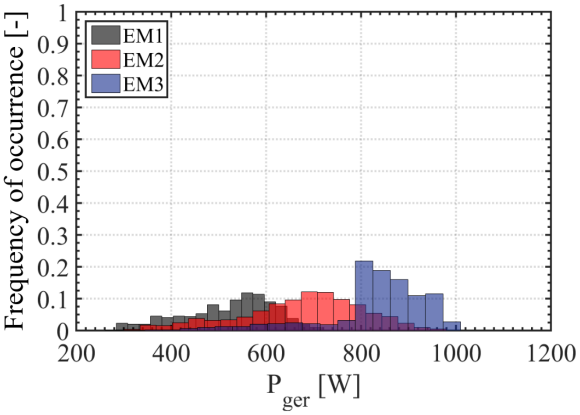

Figure 14: Frequency of occurrence of generator electric power for half charged battery.

occurrence are between 500 and 600 W and are distributed mainly to values lower than these. In the case of EM2, there is a peak around 650 and 750 W, followed by a gradual decrease for both sides. In the case of EM3, a higher frequency of values occurs between 800 and 1000 W and for smaller powers, there is a frequency distribution with very low values. The displayed behaviour of the generator power is expected. The electric power is very dependent on the rotational speed, which in turn is dependent on the sea state available power.

In Figs. 15 and 16 the battery power, P_{bat}, is illustrated. It is noted that in the case of the charged battery, the power value prevailed mostly in 50 W. This power is due to the dissipation of energy in the battery due to its internal resistance and to the fact that the battery has discharged a little during the tests of EM1 and EM2 (due to the small power available in these sea states), having the need to be charged. The negative power values, show that the battery has to supply power to the load a small part of the time in EM1 and EM2.

In the case of the half-charged battery, the battery discharges slightly on EM1 and EM2 and that the charging power was intensified with the available power of the sea state.

In Figs. 17 and 18 the frequency of occurrence of the load power, P_{load}, is shown. With the battery charged, the power of the load varies between 350 and 450 W, increasing about 30% beyond the nominal power value (360 W). It is found that this power increases with the increase of the available power in each sea state, although residually. This is due to the fact that the loads used are passive loads and they consume what the system produces so, for more energetic sea states, the power of the generator has higher values and later more power dissipation in the loads.

In the case of the half-charged battery, the load varies between 300 and 450 W, decreasing from its nominal power by about 20%. As the battery was charged, there was more power directed towards the load, while at half charge, that power had to be split into the battery and load (not forgetting that

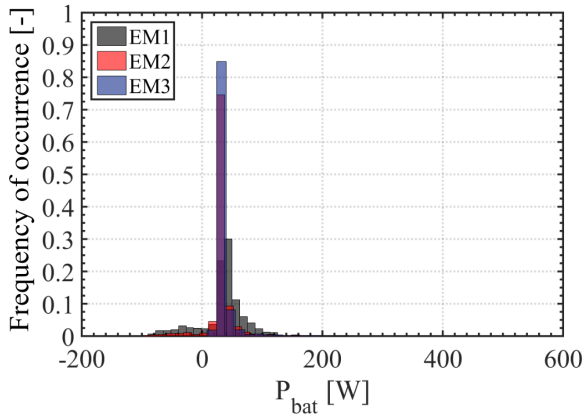

Figure 15: Frequency of occurrence of battery electric power for fully charged battery.

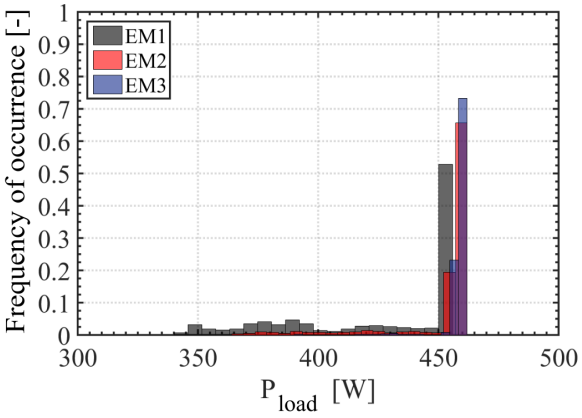

Figure 17: Frequency of occurrence of load electric power for fully charged battery.

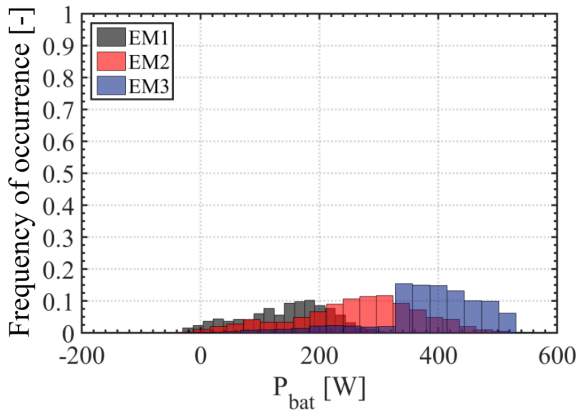

Figure 16: Frequency of occurrence of battery electric power for half charged battery.

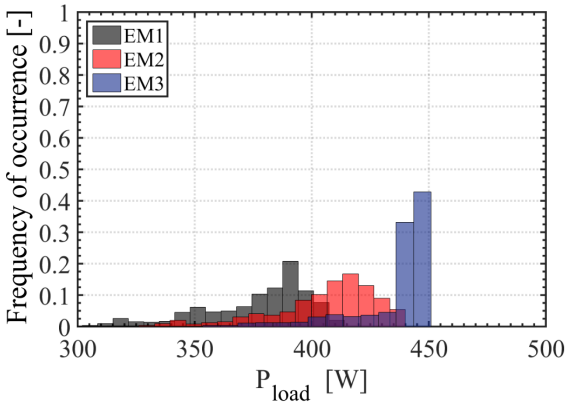

Figure 18: Frequency of occurrence of load electric power for half charged battery.

the battery acted as a buffer). With the battery fully charged, P_{load} displays higher values as the available power increases.

Figs. 19 and 20 show the occurrence frequency of the generator torque. In the case of the charged battery, for the more energetic sea states (EM2 and EM3), the torque acquires smaller values more frequently than in the less energetic sea state EM1. This is because, as the value of P_{ger} remains constant, see Fig. 13, for higher rotational speeds, the torque has necessarily to decrease. It is also found that for lower rotational speeds, as in the case of EM1, the torque has a higher frequency distribution for higher values.

On the other hand, with the battery at half charge, it is found that the torque increases with the increase in available power in the sea state. This is reflected in the fact that with the discharged battery there is a need to charge the battery and the resistive loads, thereby increasing the value of I_{ger} and T_{ger}.

Figs. 21 and 22 show the frequency of occurrence of rotational speed. With the battery charged, it is possible to see an rotational speed increase with the increase of the available power of each sea state. With the battery at half charge these values are lower than the case of the charged battery. The speed of rotation decreases because the generator torque increases in the latter situation.

4.2.2 Temporal analysis

Analysis were carried out regarding to the system operation, in order to measure its difference according to the different sea states and battery states of charge.

It was noted an increase of Δp_0, Q_{t} and P_{avai} respectively in the order of 20, 10 and 30%, consecutively between each sea state (starting at EM1, going through EM2 and ending at EM3) and that these values were independent of the state of charge of the battery.

Regarding the rotational speed, Ω, a 15% increase between each sea state was found for both cases with the battery charged and the half charged. The

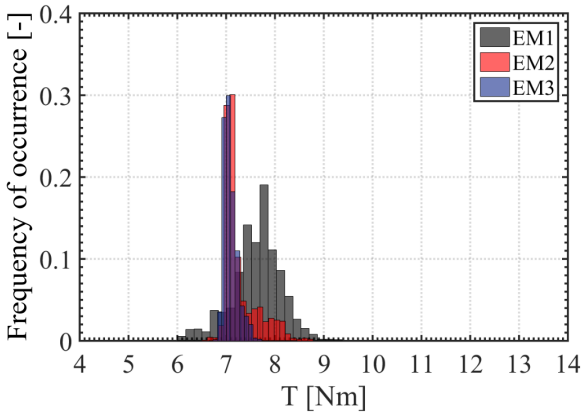

Figure 19: Frequency of occurrence of generator torque for fully charged battery.

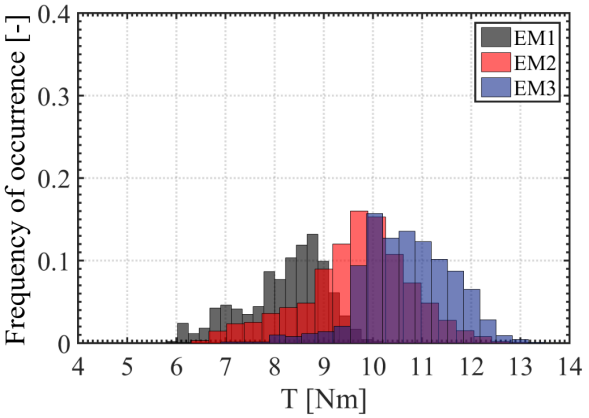

Figure 20: Frequency of occurrence of generator torque for half charged battery.

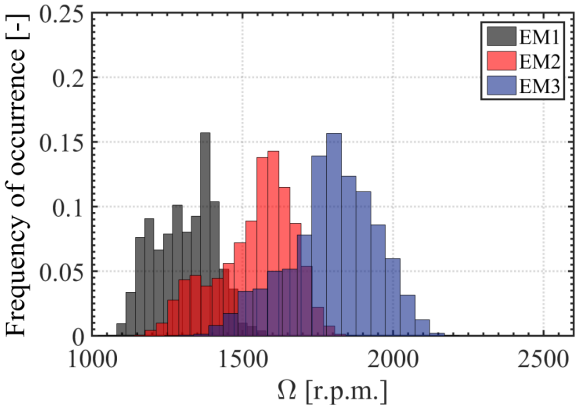

Figure 21: Frequency of occurrence of rotational speed for fully charged battery.

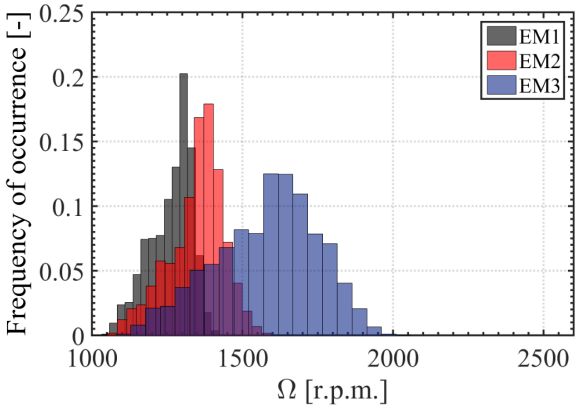

Figure 22: Frequency of occurrence of rotational speed for half charged battery.

difference between the charged and half charged battery for the same sea states was analysed and it was concluded that there was a decrease from the first to the second case by 5, 20 and 15% respectively to EM1, EM2 and EM3. This happened due to the increase of P_{ger} and consequently T_{ger}, resulting in a decrease of Ω.

Regarding the generator torque, T_{ger}, with the battery charged there was no significant variation between the three sea states, so that only between the 200 and 400 s of the EM1, values obtained were slightly higher. This is due to the fact that the battery needed to be charged, translating into higher values of P_{ger} and consequently of T_{ger}. On the other hand, with the half charged battery, there is a 15% increase between EM1 and EM2 and 10% between EM2 and EM3, translated by the increase of values of P_{avai}, P_{ger} and consequently T_{ger}. Comparing the cases of the charged and half charged battery with respect to the same sea state, there was a 5, 25 and 35% increase in the values of T_{ger} from the first to the second case, respectively to EM1, EM2 and EM3.

It is found that the mechanical power, with the battery charged, was very similar in EM1 and EM2, being slightly higher in the latter case and that there was a 20% increase from EM2 to EM3. In the case of the half charged battery, an increase of 20% from EM1 to EM2 and 25% from EM2 to EM3 was observed. On the other hand, there was a 5, 15 and 25% increase between the case of the charged and half charged battery, respectively to EM1, EM2 and EM3.

Regarding the generator electric power, P_{ger}, it was verified that with the battery charged, this value was practically equal and constant in the three sea states, so only between 200 and 400 s of EM1 the value oscillates between lower values of rotational speed. On the other hand, in the case of the half charged battery, it was found that the value of P_{ger} increased by 20% between each sea state and that in EM3 it was possible to verify the activation of the generator power limitation system from the excitation current control I_{f} and consequently from P_{ger}. Comparing the cases of the charged and the half charged battery with respect to the same sea state, there was an increase of P_{ger} from the first to the second case of 20, 30 and 40% respectively to EM1, EM2 and EM3.

It was noted that the power of the battery, P_{bat}, took residual values in the case of the fully charged battery, so that these values translated into power dissipation through the internal resistance of the battery and also in its overcharge. Values of P_{bat} in EM1 acquired 20% higher values than EM2 because there was an initial discharge of the battery followed by a subsequent charging. On the other hand, an increase of the value of P_{bat} in 10% from EM2 to EM3 was observed. In the case of the half-charged battery there was a large variation between the different sea states, whereby an increase of 50% of P_{bat} values between EM1 and EM2 and 40% between EM2 and EM3 was seen. From the integration of P_{bat} throughout the time of each test, it was concluded that in the case of the half charged battery, a charging of 9, 17 and 24% respectively was performed for EM1, EM2 and EM3.

Finally, the load power values, P_{load}, shown to be practically constant in the case of the charged battery, except in the range of 200 to 400 s of EM1 due to the low values of Ω and consequently of P_{ger}. With the half charged battery there was a 10% increase in the values of P_{load} between each sea state. Comparing the cases of the fully and half charged battery for the same sea states, it was found that the values of P_{load} decreased from the first to the second case by 15, 10 and 5% respectively to EM1, EM2 and EM3.

To conclude, the average values of the turbine efficiency, η_{turb}, generator, η_{ger}, and total, η_{total}, for different sea conditions and battery charge status were analysed. The values of η_{turb} varied from 36 to 53%, the lowest value was obtained for the EM3 with the battery charged and the highest value for the EM2 with the half charged battery. The generator had η_{ger} values between 37 and 49% and the lower and upper values were also obtained in accordance with the values of η_{turb}. Finally, the η_{total} values shown to be between 13 and 25%, with the maximum and minimum values again concordant with the previous cases.

5. Conclusions

An experimental study of a wave energy conversion system to integrate a self-powered oceanographic float was performed. The tests were carried out in the IST 55 kW turbine test laboratory, where a generator, battery and load were integrated into a test installation with an axial impulse air turbine, where a wide number of variables were measured.

It has been found that the power of the generator, P_{ger}, was extremely dependent on its rotational speed and still on the imposed resistive load. The electric powers, P_{ger}, P_{bat} and P_{load}, obtained in steady-state and variable flow conditions with charged battery and constant resistive load ($R_eq = 0.4$) were coherent with each other.

The battery was found to act as a buffer when there were generator current peaks caused by the increase in its rotational speed. Therefore, it is essential to use a battery in this kind of systems in order to attenuate such peaks or make use of a DC-DC converter in order to control the current that

goes to the load.

It was found that the battery was often charged above its rated voltage (12 V). Due to this, by analysing the values of P_{bat} in steady-state and variable flow conditions with the charged battery, it was possible to observe the overcharge of the battery. This problem can be overcome by using a DC-DC converter between the generator and the battery, where the charging voltage of the battery is limited to 12V.

It was found that with the battery almost discharged, it did not have enough power to initially power the excitation system of the generator, so with the increase of the rotational speed of the turbine, the generator enters in runaway conditions, without torque and power production.

In variable flow conditions, it was verified that the behaviour of the generator was extremely influenced by the state of charge of the battery and also by the available power each sea state. Variables such as P_{ger}, P_{bat}, P_{load}, T_{ger}, and P_{mec} were shown to be higher when the battery was half charged, while Ω was higher with the battery fully charged. With the battery half charged, the variables P_{ger}, P_{bat}, P_{load} and T_{ger}, were found to be extremely dependent on the rotational speed, while with the battery fully charged, the values were practically constant and dependent on the available power of each sea state.

6. Future work

Due to the operation of the used electric circuit, it is suggested to incorporate a DC-DC converter between the generator and the battery and between the generator and the load, in order to avoid the overcharge of the battery and current peaks in the load. The adoption of a storage system with batteries with higher capacity or a parallel scheme should be studied. In addition, other battery technologies, particularly the deep cycle ones, should be studied. In addition, it is advisable to use loads with self-adjusting capacity, so that their power consumption is always the nominal, which was not verified in the tests performed.

In order to be able to compare the generator tested here and new types of machines, namely other synchronous, direct current and induction generators, it is advisable to carry out later experimental tests and analysis for the same conditions studied here.

Finally, if we continue to evaluate the alternative studied here (car alternators), it is advisable to remove the internal voltage regulator from the generator and to develop a new one that meets the optimal control of its power and torque for the operating conditions of the turbine.

Acknowledgements

The research was partially funded by the Portuguese Foundation for Science and Technology (FCT) through WAVEBUOY project - Wave-powered oceanographic buoy for long term deployment - PTDC/MAR-TEC/0914/2014.

References

[1] Action plan for a maritime strategy in the atlantic area. https://eur-lex.europa.eu. Accessed on 6 january, 2018.

[2] J. C. C. Henriques, A. F. O. Falcão, R. P. F. Gomes, and L. M. C. Gato. Air turbine and primary converter matching in spar-buoy oscillating water column wave energy device. In *Proceedings of the 32nd International Conference on Ocean, Offshore and Arctic Engineering, OMAE 2013*, Nantes, France, June 2013.

[3] A. F. O. Falcão. Wave energy utilization: A review of the technologies. *Renewable and Sustainable Energy Reviews*, 14(3):899 – 918, 2010.

[4] A. F. O. Falcão and L. M. C. Gato. Turbine with radial inlet and outlet rotor for use in bidirectional flows, Feb. 15 2011. US Patent App. 13/580,099.

[5] A. A. D. Carrelhas. Estudo experimental do modelo e do protótipo de uma turbina autoretificadora bi-radial com pás fixas. Master's thesis, IST, Universidade de Lisboa, 2017.

[6] S. Dixon and C. Hall. Chapter 6 - three-dimensional flows in axial turbomachines. In S. Dixon and C. Hall, editors, *Fluid Mechanics and Thermodynamics of Turbomachinery (Seventh Edition)*, pages 215 – 263. Butterworth-Heinemann, Boston, seventh edition edition, 2014.

[7] G. Marques and M. J. Resende. Sebenta de Circuitos Elétricos - Sistemas Elétricos e Electromecânicos , 2009.